Energy Conversion and Management 309 (2024) 118424

Contents lists available at ScienceDirect

Energy Conversion and Management

journal homepage: www.elsevier.com/locate/enconman

Research Paper

Operational, economic, and carbon footprint feasibility of a moderately-high-temperature heat pump as an alternative to conventional boilers in various scenarios

Ghad Alarnaot Alarnaout, Joaquín Navarro-Esbrí, Adrián Mota-Babiloni *

ISTENER Research Group, Department of Mechanical Engineering and Construction, Universitat Jaume I, Castelló de la Plana, E-12071, Spain

ARTICLE INFO

Keywords:
District heating network
District cooling network
Low GWP
Carbon footprint analysis
Energy performance

ABSTRACT

This article conducts a comprehensive theoretical analysis containing operational, carbon footprint, and economic aspects of a medium–high temperature heat pump (HP) employing R-1234ze(E) as working fluid. Different scenarios consider three types of heat pump connections with district heating and cooling (DHC) networks. The study contains a total of six scenarios, where the first (single stage/two stage cascade (SS/TSC)) and second (SS) scenarios use waste heat for district heating. The third (SS/TSC) and fourth (SS) scenarios produce heating and cooling for district heating and cooling. The fifth (SS) and sixth (TSC) scenarios use heat from the district heating network (DHN) for conventional boiler applications (process heating). Regarding the energy analysis, the internal heat exchanger (IHX) presents a positive impact across all scenarios, improving from 1.5 to 4.6%. Moreover, the TSC configuration exhibits a lower coefficient of performance (COP) than SS for scenario 1 (−20.1%), and for scenario 3 exhibits higher COP than SS (+3.7%). The R-1234ze(E) COP for most scenarios surpasses R-134a. The second scenario, characterized by a lower condensing temperature, results in the highest COP (5.94), due to presenting the lowest compression ratio among the six scenarios. From a carbon footprint perspective, all scenarios demonstrate lower emissions with R-1234ze(E) than R-134a, with the second scenario exhibiting the lowest emissions (358 tCO_2e), which is attributed to its low energy consumption. Compared to a natural gas boiler, the second scenario achieves an 84.4% reduction in emissions. Regarding the economic analysis, TSC configurations exhibit higher costs than SS ones (+59% for scenario 1 and +51% for scenario 3). The first (SS) and second scenarios present the lowest capital expenditure (CAPEX), 35161 € and 37717 € respectively, with the second scenario having the least operating expenditure (OPEX), 25275 € due to its low energy consumption, making it a viable alternative to the boiler. Economic viability analysis reveals that only the first four scenarios with SS configuration are feasible, given their OPEX is lower than the boiler, in the case of scenarios 1 and 2 (−14% and −40%), and lower than boiler plus chiller in the case of scenarios 3 and 4 (−18% and −40%). For only heating, the second scenario exhibits the lowest payback period (PBP) (2.18 years), and for heating and cooling, the fourth exhibits the lowest PBP (1.94 years) over a fifteen-year life cycle.

1. Introduction

Humanity confronts climate change as a significant global challenge, encompassing notable and enduring alterations in Earth's climate patterns. The residential sector's heating and cooling demand in Europe accounts for approximately 50% of the final energy usage [1]. Moreover, one-third of the European Union's energy-related greenhouse gas (GHG) emissions originate from buildings, with 80% of the energy consumed dedicated to heating, cooling, and hot water. The Energy Performance of Buildings Directive (EPBD) plays a pivotal role in directly advancing the European Union's energy and climate objectives. The directive aims to achieve fully decarbonized buildings by 2050 [2].

The technology of district heating and cooling (DHC) has been acknowledged as a viable solution to reduce primary energy consumption due to its capacity of the decarbonization heating and cooling sector using renewable energies, the same with local emissions, allowing using local resources; therefore, this system adapts the heating and cooling requirements of buildings [2]. The fundamental operation of DHC consists of a centralized building (generation system) that, through a network pipeline (distribution system), provides heating for domestic hot water (DHW), process heating (PH), and space heating (SH)

* Corresponding author.
E-mail addresses: al376107@uji.es (G. Alarnaot Alarnaout), navarro@uji.es (J. Navarro-Esbrí), mota@uji.es (A. Mota-Babiloni).

https://doi.org/10.1016/j.enconman.2024.118424
Received 29 January 2024; Received in revised form 21 March 2024; Accepted 10 April 2024
Available online 22 April 2024

Nomenclature

A	Area (m^2)
C	Cost (€)
I_o	Initial investment (€)
LMTD	Logarithmic Mean Temperature Difference (K)
$\dot{Q}$	Heat transfer (kW)
r	Discount rate
T	Temperature (°C or K)
U	Overall heat transfer coefficient (kW m^{-2} K^{-1})
Wc	Compressor power consumption (kW)
CAPEX	Capital expenditure (€)
CF	Cash inflow (€)
NPV	Net present value (€)
OPEX	Operating expenditure (€)
PBP	Payback period (years)

Greek symbols

Δ	Variation
α	Refrigerant recycling factor
β	Indirect emission factor ($kgCO_2e$ kWh^{-1})

Subscripts

cond	Condenser
disc	Discharge
evap	Evaporator
HX	Heat exchanger
k	Condensation
o	Evaporation
source	Heat source
t	Annual
vol	volumetric

Abbreviations

ASHP	Air source heat pump
Ch	Chiller
CHP	Combined heat and power
CHX	Cascade heat exchanger
COP	Coefficient of performance
CPI	Consumer price index
DCN	District cooling network
DHC	District heating and cooling
DHN	District heating network
DHW	Domestic hot water
EPBD	Energy Performance of Buildings Directive
GHG	Greenhouse gas
GWP	Global warming potential
HFO	Hydrofluoroolefin
HP	Heat pump
HT	High temperature
HTHP	High-temperature heat pump
IHX	Internal heat exchanger
IRR	Internal rate of return
LT	Low temperature
PC	Process cooling
PH	Process heating
Sc	Scenario
SC	Space cooling
SH	Space heating
SS	Single stage
SV	Suction volume
TCO	Total cost of ownership
TEWI	Total equivalent warming impact
TSC	Two-stage cascade

(consumption system) [3]. Additionally, it offers cooling for space cooling (SC) and process cooling (PC). The thermal fluid circulating inside the pipeline is water.

Throughout history, the district energy system has undergone transformations, leading to the development of five generations. The initial generation (1G), prevailing from 1880 to 1930, was composed of conglomerates of industries and complexes with high energy consumption. Their operation relied on the combustion of coal or other fossil fuels in thermal power plants, generating heat and electricity. The distribution fluid was high-temperature and high-pressure steam operating at temperatures between 120 to 200 °C. This steam was produced through coal-waste steam production plants, and the energy was distributed to various remote customers through storage systems from a centralized generation plant.

Subsequently, the second generation (2G), covering from 1930 to 1980, marked a departure from the first by introducing pressurized hot water systems. In this generation, fossil fuels were still being used; however, it allowed for the incorporation of technologies such as cogeneration, enabling the simultaneous production of heat and electricity from a single fuel source. These systems operated at temperatures between 120 and 160 °C.

With technological progress, the third generation (3G) of district heating systems emerged between 1980 and 2020. The most notable aspect of this generation is the integration of renewable energy technologies, including geothermal, solar thermal, biomass, and waste. This renders district heating networks more environmentally friendly, effectively reducing greenhouse gas emissions and improving sustainability. Additionally, this generation incorporates improved monitoring capabilities and construction techniques, presenting improved thermal insulation. These advancements have facilitated the attainment of lower operating temperatures, ranging from 70 to 100 °C [4].

The fourth and fifth generations have evolved from the third generation [5,6]. The fourth generation (4G) operates with temperatures between 35 to 70 °C, whereas the fifth generation (5G) operates between 10 to 35 °C. These novel categories function at lower temperatures to minimize heat loss and can be integrated into modern power supply systems. They are also compatible with various heat sources [3]. This capability enables modern district systems to harness renewable energy sources, capture waste heat, and connect with heat pumps (HPs) in diverse configurations. Detailed descriptions of these configurations can be found assessed by Barco-Burgos et al. [3]. These advancements offer notable advantages, including (i) reducing dependence on fossil fuels and mitigating greenhouse gas emissions through the utilization of renewable energy sources and the recovery of waste heat; (ii) improving energy efficiency by harnessing waste heat from industrial processes and power generation; (iii) facilitating the transition toward more sustainable and climate-resilient energy systems [3].

Due to measures implemented to combat climate change, particularly global warming, HPs have garnered global attention. This is attributed to the fact that when HPs consume energy, they provide a coefficient of performance (COP) ranging between 3 and 6, coupled with the capacity for energy recovery [7]. HPs allow the recirculation of environmental and waste heat into a heat production process. As a result, a system appears that not only demonstrates energy efficiency but also represents an environmentally friendly solution for heating and cooling applications across various domains [8]. HPs play a pivotal role in significantly reducing GHG emissions, with a particular emphasis on mitigating CO_2 emissions.

Regarding refrigerants, Mateu-Royo et al. [9] conducted a comparative analysis between HPs and gas boilers for moderately-high-temperature applications using R-1234ze(E) under various conditions. Their study revealed that HPs facilitated a notable reduction in emissions, achieving a maximum 78% emissions decrease compared to gas boilers. Xiao et al. [10], concluded that R-1234ze(E) offers a favorable combination of thermodynamic, environmental, and safety properties specifically suited for solar district heating systems. Notably, R-1234ze (E) exhibits thermodynamic properties similar to R-134a with much lower global warming potential (GWP), making it suitable for moderately high-temperature applications. Furthermore, it is classified as group A2L, which is non-toxic and moderately flammable [9].

High-Temperature Heat Pumps (HTHPs) can be integrated into district heating systems, exhibiting a COP within the range of 2–6 or 2–8 under specific conditions [3]. In a study conducted by Mateu-Royo et al. [11], an examination of HTHPs integration involved a comparison of various refrigerants with R-134a, utilizing the district heating network (DHN) as the heat source. This approach can yield a notable reduction of up to 98% in CO_2e emissions in Sweden, particularly when compared with conventional natural gas boilers. Consequently, the collaborative deployment of HTHPs alongside DHN signifies a notable improvement in climate change mitigation. It reflects a positive perspective on utilizing sustainable energy conversion technologies [11]. Nevertheless, HTHPs still have some existing limitations, such as temperature range, low efficiency, and high economic cost [12]. The most important limitations are the market and the compressor. On the one hand, implementing HTHPs requires confronting the high economic costs and the customer's interest in integrating HTHPs, especially considering the availability of low-cost boiler gas, which is more attractive than HTHPs. On the other hand, most of the challenges of HTHPs lie in the compressor; in high temperature (HT) conditions, the compressor works at higher pressures, and the discharge temperature limits the sink temperature; in addition to this, those conditions require higher cooling for the compressor [13]. Therefore, a HTHP with an appropriate price-efficiency ratio is required to catch the market's attention.

As mentioned before, HP can harness waste heat, and many processes, such as industrial processes, generate waste heat. The efficient management of waste heat generated in industrial processes is crucial to more sustainable and cost-effective practices. As industries conduct their operations, a significant percentage of heat is dissipated as waste, presenting a valuable opportunity for resource optimization. The magnitude of this thermal loss varies across sectors and often reaches essential percentages. The underutilization of this source of thermal energy not only causes an economic loss but also carries a considerable environmental impact. In this context, the capture and efficient utilization of waste heat emerges as fundamental strategies to promote industrial sustainability, reduce operating expenditure (OPEX), and mitigate environmental footprints [14].

A few papers have investigated district heating and cooling networks with heating and cooling production methods and connected to different consumptions under several assumptions. Also, they compared the emissions to conventional natural gas boilers. The sustainability of DHN and district cooling network (DCN) can be improved by connecting high-efficiency electrically-driven heat pumps that can be optimized for different scenarios. This way, these scenarios need to be explored and compared, depending on the generation, the type of integration of the heat pumps, its configuration and the fluid refrigerant to be used. DHN and DCN networks incorporating heat pumps are a promising alternative to conventional boilers that use fossil fuels and chillers with direct ambient condensation. However, to capture the market's interest and advance in the state-of-the-art, sustainable heat pumps connected to those systems need to be studied and developed to be economically and technically feasible. In this paper, a wide range of specific conditions never explored before of heat pumps integrated into DHN (two of them DHC) are proposed and analyzed their operational and economic feasibility. Also, a carbon footprint analysis is done compared to the conventional boiler for heating and a chiller for cooling and obtain a multi-parameter and comprehensive approach. Among the different types of connections of heat pumps to DHC explored, three were selected and adapted to the six conditions based on using waste heat, heating and cooling production, and boosting DHN temperature. To explore its feasibility, HTHP is employed for higher sink temperatures in DHN in some conditions. This paper contributes to promoting heat pumps in DHC networks to achieve higher energy efficiency, lower carbon footprint, and higher economic feasibility. This leads to an attractive replacement of low-cost natural gas boilers, particularly in the DHC context. Additionally, it expands research domains in integrating heat pumps in DHC networks. As a result, this study aims to investigate the potential viability of a moderately-high-temperature heat pump employing R-1234ze(E) into DHN or DHC in conditions in which the system can result with a high energy efficiency. This is done through a compressive analysis of six distinct scenarios, considering various applications of heat pumps in DHC. The research aims to assess each scenario's operational, carbon footprint, and economic feasibility. The carbon footprint and economic feasibility are compared to conventional natural gas boilers that use fossil fuels to study the potential of HPs replacing boilers.

2. System description

2.1. Research scenarios

For this study, the single stage (SS) and two stage cascade (TSC) cycles, both with an internal heat exchanger (IHX), will be considered; in the SS configuration, the main components are the evaporator, the condenser, the compressor, and the expansion valve. In the TSC configuration, the main components are the evaporator, the condenser, two compressors, two expansion valves, and a cascade heat exchanger (CHX). The cycle will be integrated into DHN and, in some configurations, also with the DCN. There will be three primary configurations of integrating HPs in the DHC systems.

Fig. 1 shows the first configuration, the central heat pump connected to district heating (C_HP_DHN). In this configuration, the HP is positioned within the central generation system, utilizing low-grade heat (coming from industrial process cooling) as the primary heat source for evaporating the refrigerant. Whereas the heat sink of the HP, the condenser uses the return line of DHN to elevate the temperature of the water and inject it into the supply line, providing heat to the DHN. Central HPs with a single heat source must possess adequate thermal capacity to comprehensively meet the year-round heating requirements. Centralized HPs can function independently or integrate into a system with other equipment, such as Combined Heat and Power (CHP) or harness waste heat, improving flexibility [3].

Fig. 2 illustrates the second configuration, which focuses on a central heat pump integrated with district heating and district cooling systems. This setup is designed for concurrent heating and cooling generation for DHC networks. In this configuration, the heat source utilizes the thermal energy present in the water from the return line of the DCN to evaporate the refrigerant. Subsequently, the water temperature is lowered and reintroduced into the supply line of the DCN. Regarding the heat sink, the process remains analogous to that of the first configuration.

Fig. 3 shows the last configuration, the local heat pump connected to DHN (L_HP_DHN); in this case, the heat pump is locally placed and serves as a booster in the DHN. It utilizes the DHN supply line as the heat source for evaporating the refrigerant. [3].

This study considers six scenarios, each with its conditions, applications, and configurations, as illustrated in Table 1. Given the differences between the evaporation temperature (T_o) and condensing temperature (T_k) in those scenarios, if the scenario presents an acceptable pressure ratio, only SS will be used; if it presents a moderate pressure ratio, then it will be examined with SS and TSC; if it presents a high-pressure ratio, then only TSC will be used.

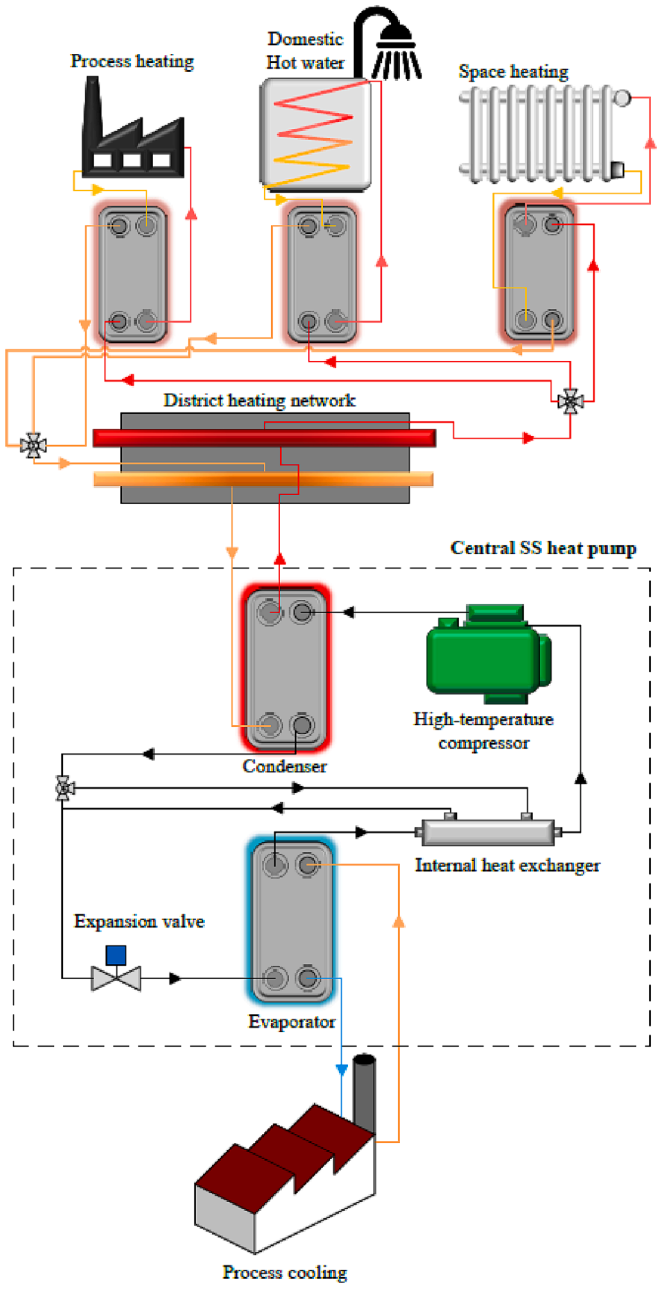

Fig. 1. Central heat pump connected to DHN (C_HP_DHN).

The initial scenario involves capturing waste heat from an industrial process by cooling dissipation water and substituting the conventional boiler for heat provision. In executing this process, the evaporator utilizes water as a heat source for evaporating the refrigerant, reducing the disparity between T_o and T_k. This adjustment improves HPs efficiency. Subsequently, the condenser (acting as a heat sink) facilitates heat transfer, providing heat to 4G DHN. In this instance, the scenario will contain two configurations: the SS cycle and the TSC. The second scenario closely resembles the first, with the distinction that, in this case, the heat pump operates with a condensing temperature of 65 °C, and only the SS cycle is considered in this case.

The third scenario involves the simultaneous heat and cooling production for injection into a 4G DHC system. In the DHN, water from the network enters the condenser (heat sink) with inlet and outlet temperatures of 40 °C and 70 °C, respectively. Similarly, in the DCN with the evaporator, water from the DCN enters the evaporator with inlet and outlet temperatures of 17 °C and 7 °C, respectively. Additionally, this

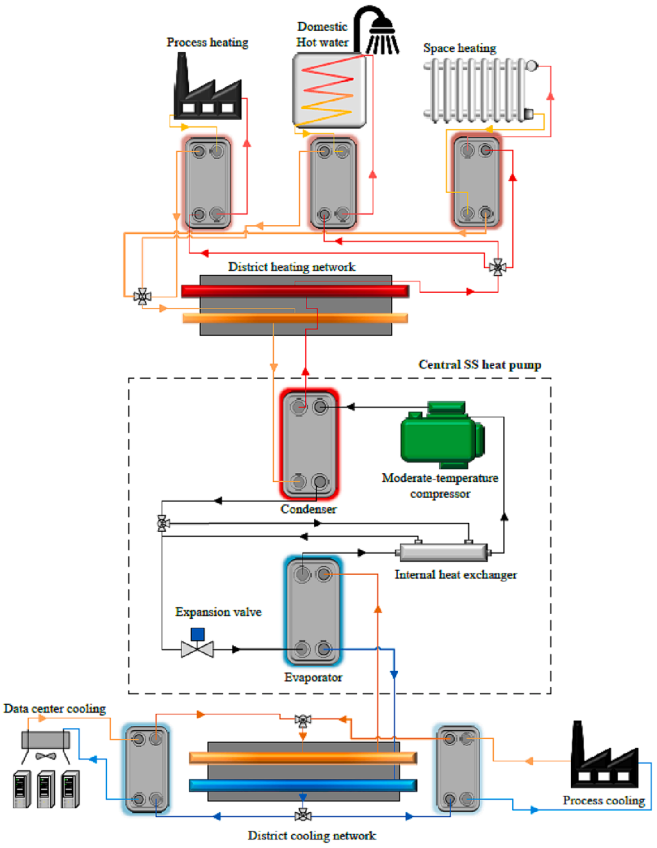

Fig. 2. Central heat pump connected to DHC (C_HP_DHC).

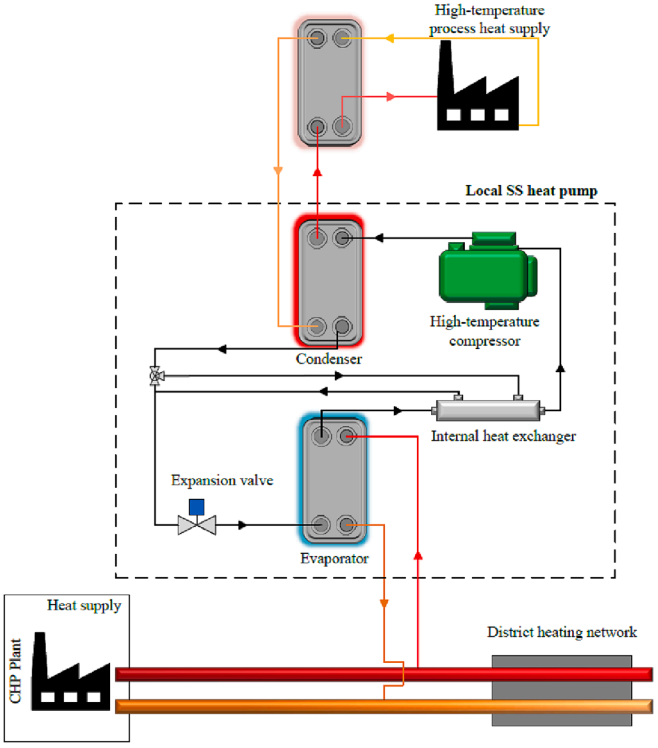

Fig. 3. Local heat pump connected to DHN (L_HP_DHN).

Table 1
Scenarios considered for the study.

Scenarios	T_o (°C)	T_k (°C)	Configuration of cycle	Process	Configuration of the connection
Scenario 1	30	80	SS/TSC	Industrial (cooling dissipation water) and heat supply (conventional boiler substitute) supply heat to 4G District Heating Network (DHN).	C_HP_DHN
Scenario 2	30	65	SS	Cooling dissipation water (heat recovery) and supply heat to 4G District Heating Network (DHN).	C_HP_DHN
Scenario 3	2	65	SS/TSC	Simultaneous production of DHN heating (70–40 °C) and DCN cooling (17–7 °C) 4G.	C_HP_DHC
Scenario 4	2	45	SS	Simultaneous production of DHN heating (47–40 °C) and DCN cooling (17–7 °C) 4G.	C_HP_DHC
Scenario 5	50	90	SS	Heat production (conventional boiler substitute) sourced from DHN (70–40 °C) 4G.	L_HP_DHN
Scenario 6	10	90	TSC	Heat production (conventional boiler substitute) sourced from DHN (<40 °C) 5G.	L_HP_DHN

scenario will be investigated using the SS cycle and the TSC. The fourth scenario is similar to the third one, with two differences: the condensation occurs at 45 °C, and the outlet water temperature from the condenser is 47 °C. For this case, only SS configuration is considered.

The fifth scenario involves harnessing heat from the supply line of DHN for heat production. The water entering from the DHN flows into the evaporator (heat source) with inlet and outlet temperatures of 70 °C and 40 °C, respectively, and the connection is decentralized. Also, in this case, only SS configuration is considered. The sixth scenario mirrors the process of the fifth. However, in this case, the investigation focuses on the fifth-generation DHN with a heat source temperature (T_{source}) below 40 °C. Notably, this scenario will exclusively employ the TSC configuration due to the high difference between T_o and T_k. For this study, Figs. 1, 2, and 3 show the heat pump schematic for SS configuration.

For the TSC configuration, Fig. 4 presents the schematic diagram of the heat pump. In this instance, the primary working fluid is R-1234ze (E), which is employed in the high-temperature circuit. R-1234yf is utilized as the working fluid for the low-temperature circuit due to its advantageous thermodynamic and safety properties.

R-1234ze(E) has been chosen as the primary working fluid for the six scenarios due to its favorable thermodynamic and safety properties, particularly in DHN. Additionally, its potential in HPs as an alternative to conventional boilers is notable. Table 2 presents the main characteristics of the working refrigerants.

3. Methodology and modelling

The system modelling strategy, assumptions, and boundary conditions are presented in this section.

3.1. System modelling

Fig. 5 illustrates the steps employed for the theoretical operation. Refrigerant specifications, boundary conditions, and assumptions will be incorporated as input parameters in the Engineering Equation Solver (EES) [15]. This software contains all the necessary equations to simulate the thermodynamic cycle. Once the output parameters are obtained, a commercial component will be chosen for each constituent of the cycle. The criteria for selecting commercial components are guided by the results obtained for each component.

3.2. Calculation method and compressor modelling

The calculation methodology of the operational parameters, such as COP and compressor efficiency, is based on manufacturer data [16]. The simulation is made using the manufacturer's software [17]. The conditions of each scenario are applied to the software to obtain the operational parameters of each scenario and develop the paper. To calculate the COP, the load at the condenser is set at 100 kW for each scenario. Consequently, the COP depends directly on compressor power consumption. As a result, the compressor modelling has to be validated.

An SS HP prototype at the laboratory that employs a compressor from the same manufacturer is used to validate the compressor and

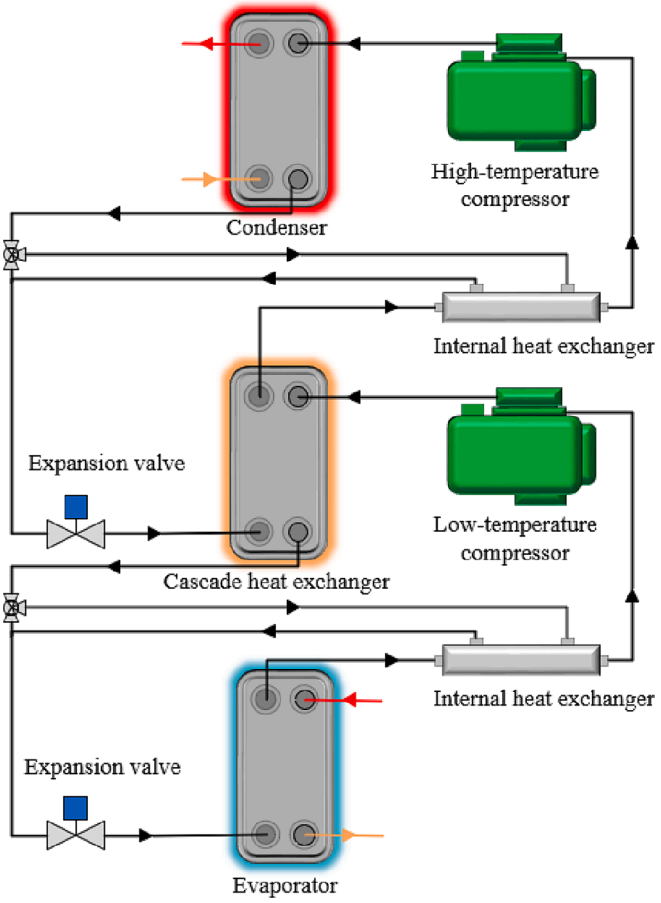

Fig. 4. Scheme of TSC configuration.

Table 2
Main characteristics of R-1234ze(E), R-1234yf, and R-134a.

Parameters	R-1234ze(E)[a]	R-1234yf[b]	R-134a[c]
Molecular formula	$CF_3CH{=}CHF$	$CH_2{=}CFCF_3$	CH_2FCF_3
Molecular weight (g mol^{-1})	114	114	102
Critical temperature (°C)	109.4	94.7	101.06
Critical pressure (bar)	36.36	33.8	40.59
Critical density (kg m^{-3})	489	475	511
Normal boiling point (°C)	−18	−21	−25
Normal freezing point (°C)	−156	−150	−96
Ozone Depletion Potential (ODP)[d]	0	0	0
Global warming potential (GWP)[e]	6	4	1300
ASHRAE Std. 34 Safety Classification[d]	A2L	A2L	A1

[a] [29].
[b] [30].
[c] [31].
[d] [32].
[e] [22].

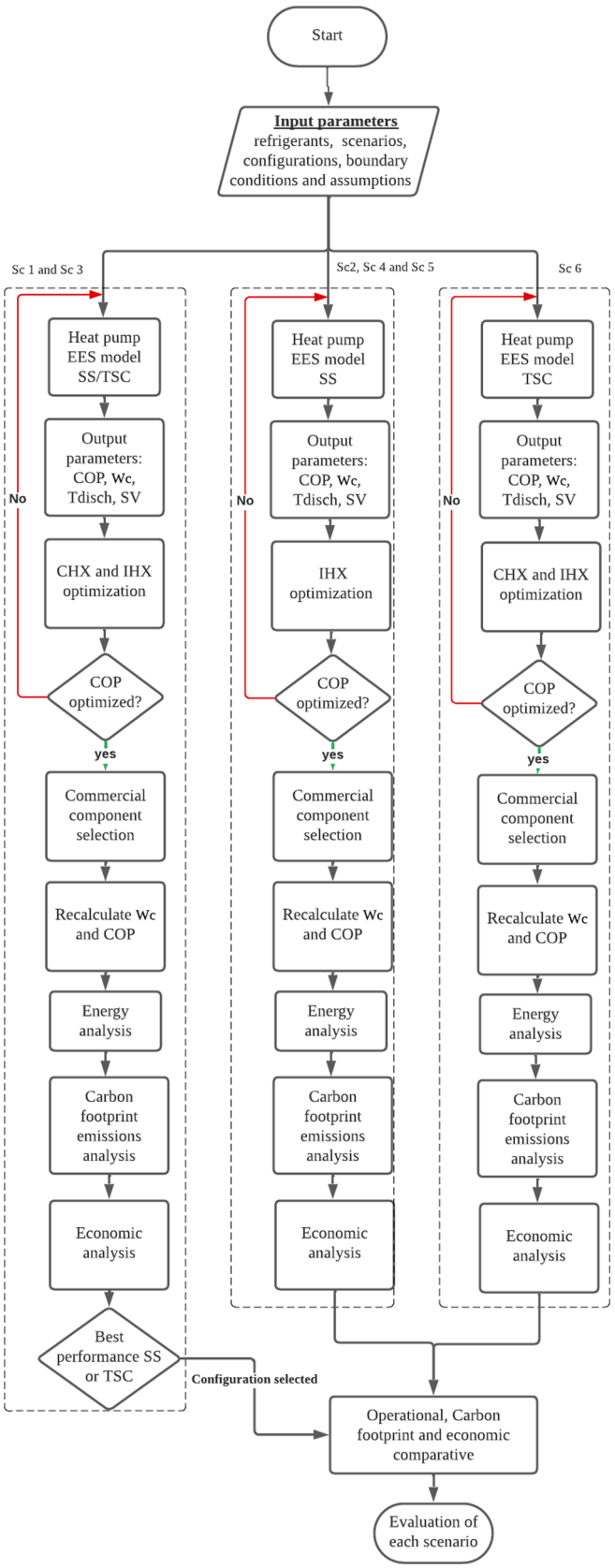

Fig. 5. Flow diagram for the modelling cycle with IHX.

evaluate its working conditions. Only SS configurations are experimented due to the laboratory limitations. Once the results are obtained, the actual compressor power consumption of the laboratory HP will be compared to the power consumption of the same compressor obtained from the manufacturer's software. Fig. 6 shows the deviation of the actual power consumption obtained using the laboratory HP from that obtained using manufacturer software. The observed deviations are because the HP prototype is not optimized for the operational conditions, the error of the sensors, and irreversibilities such as additional pressure drop and thermal losses.

The maximum deviation observed is 6%, and the minimum is 2%. These results show that the operational parameters given by the manufacturer software are valid for this paper, as shown in Fig. 6.

3.3. Assumptions and boundary conditions

Two parameters, T_o and T_k, are primarily employed to simulate the operating conditions. Table 3 outlines all the conditions established for all scenarios. Additionally, the following boundary conditions are considered: (i) Neglecting pressure losses in the pipes and internal components of the circuit. (ii) Ignoring heat losses from the system compared to other energy changes. (iii) Assuming isenthalpic flow through the expansion valve in the compression cycle. (iv) The actual power consumption of the compressors is determined based on the data provided by the manufacturer, specifying the condensation, evaporation, and superheat conditions of each scenario [9].

The scenarios' cycles are delineated by the utilization of the working fluid. Fig. 7a) illustrates the cycle for each scenario employing R-1234ze (E). Notably, the cycles for Sc2 and Sc3 TSC HT are identical. Furthermore, Fig. 7a) represents the HT circuit for the TSC configuration, whereas Fig. 7b) depicts the low temperature (LT) circuit's cycle using R-1234yf. Finally, Fig. 7c) displays the cycles for R-134a. In this instance, the TSC configuration is exclusively represented for LT, given that the comparative analysis involves R-1234ze(E) operating with R-1234yf compared to R-1234ze(E) operating with R-134a.

4. Results and discussion

This section contains three analyses. Firstly, an operational analysis will be conducted on the six scenarios, comparing their pressure ratio, discharge temperature, and COP and examining the influence of the IHX. Additionally, a comparative assessment between R-1234ze(E) and R-134a will be initiated to evaluate the potential of R-1234ze(E) as a low GWP refrigerant. For the TSC comparison, the process is done using R-134a instead of R-1234yf.

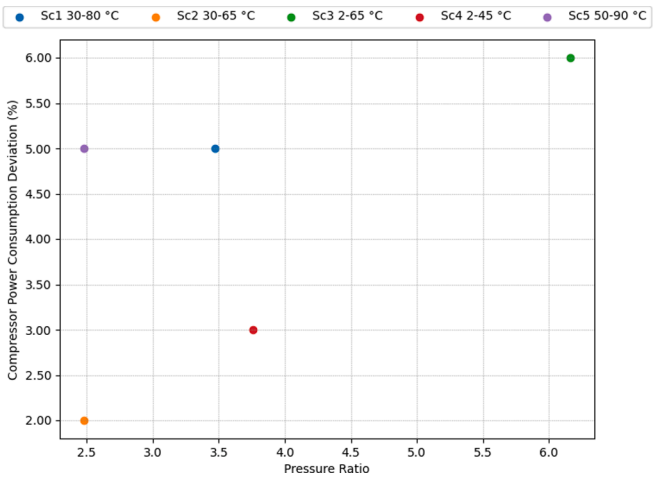

Fig. 6. Deviation of laboratory compressor power consumption from compressor manufacturer's software.

Table 3
Conditions and assumptions for every scenario.

Parameter	Assumed value
Superheating degree	10 K (7 K TSC scenario 1)
Subcooling degree	2 K
Cascade heat exchanger temperature difference	5 K
Thermal power of condenser for every scenario ($\dot{Q}_k$)	100 kW

Secondly, a carbon footprint analysis will be performed utilizing the Total Equivalent Warming Impact (TEWI) to compare R-1234ze(E) with R-134a and compare heat pump emissions (working with R-1234ze(E)) with those of conventional boilers. This analysis aims to provide observations into the environmental implications of adopting heat pumps compared to traditional boiler systems.

Finally, an economic analysis will be executed to compare the feasibility of HP with conventional boilers. This economic evaluation aims to comprehensively understand the economic viability of using heat pumps instead of traditional boiler systems.

4.1. Operational analysis

Fig. 8 shows the pressure ratio of each scenario for R-1234ze(E) compared to R-134a. Apart from cascade circuits, scenario 2 presents the lowest pressure ratio among the six scenarios, which is the most promising scenario for energy performance. Regarding the refrigerants comparative, Fig. 8 shows that R-134a presents a higher pressure ratio for low pressures than R-1234ze(E), whereas R-1234ze(E) presents a higher pressure ratio for high pressures. This phenomenon occurs due to the difference in the thermodynamic properties between the refrigerants.

Fig. 9 shows the discharge temperature of each scenario for R-1234ze (E), R-134a, and R-1234yf with IHX activated to observe the maximum discharge temperature. Scenarios 5 and 6 present the highest discharge temperature due to its condensing temperature (90 °C), reaching 110.2 and 110.5 °C respectively. When it comes to refrigerants comparison, R-134a reaches higher temperatures discharge than R-1234ze(E) or R-1234yf. R-134a presents higher vapor enthalpy than R-1234ze(E), and R-1234yf, therefore, reaches higher discharge temperatures. Those results are similar to the results conducted by Mateu-Royo et al. [11]; despite the difference in the heat sink and heat source temperatures between their paper and this paper, both papers show that R-134a

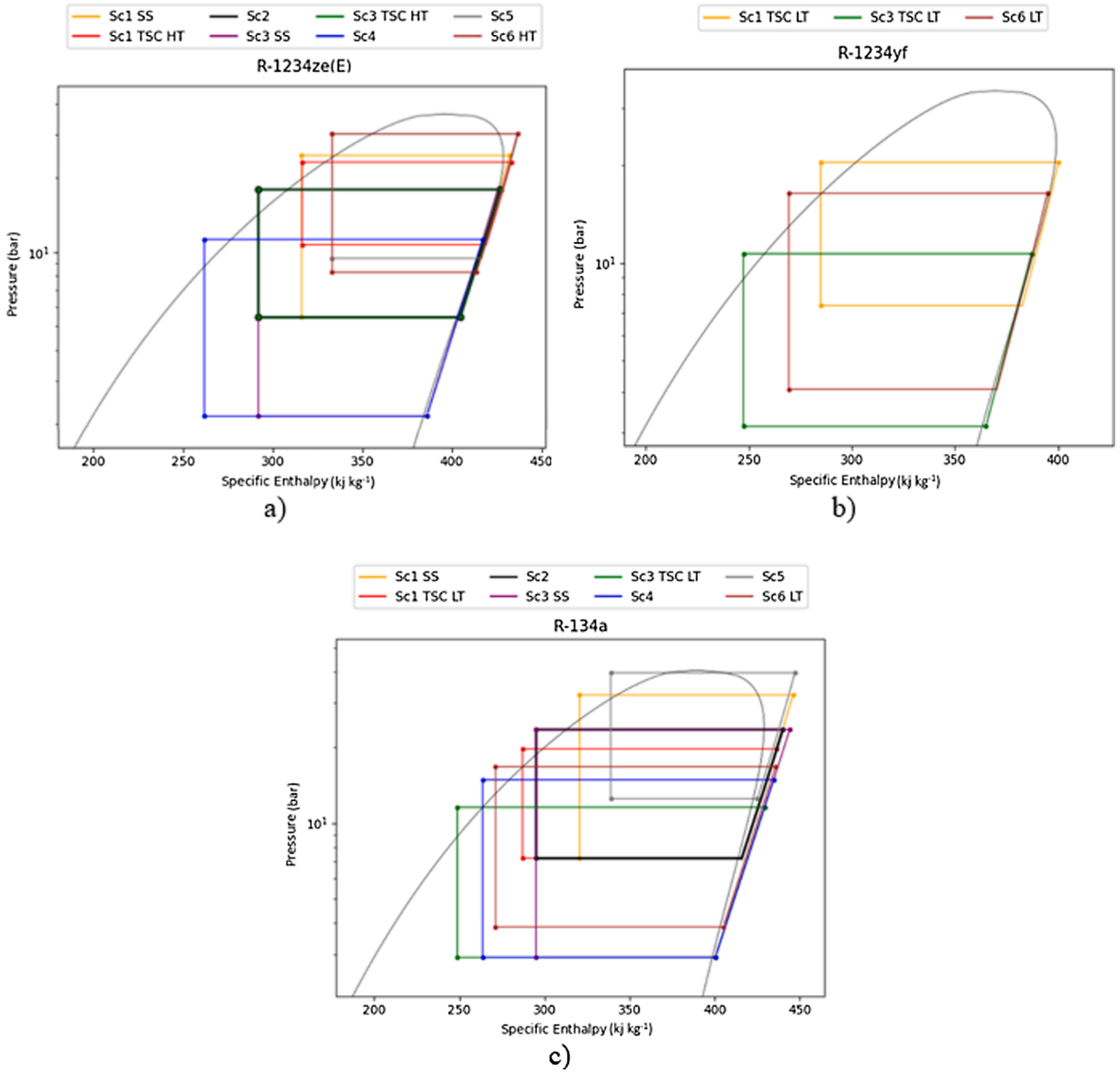

Fig. 7. P-h diagram cycles of a) R-1234ze(E), b) R-1234yf, and c) R-134a.

presents higher discharge temperatures and also show that the higher the pressure ratio is, the higher is the discharge temperature, this case can be observed when scenario 2 and 3 are compared.

Regarding COP, Fig. 10 illustrates a comparison between scenarios with and without an IHX for R-1234ze(E), the same with Fig. 11 for R-134a. Scenario 2 exhibits the highest COP among the six scenarios. This outcome is attributed to scenario 2 having the smallest disparity between the condensing temperature (T_o) and the evaporating temperature (T_k) compared to the other scenarios, signifying a lower power demand for the compressor.

The inclusion of the IHX positively impacts COP across all scenarios, particularly in scenarios with a more significant T_o-T_k differential, as observed in scenarios 1 and 3. Notably, this improvement in COP has an upper limit to prevent exceeding the compressor's maximum discharge temperature for each scenario. Also, in this case, similar conclusions are obtained by Mateu-Royo et al. [11]; nevertheless, in this paper, the percentage of improvement is lower due to the IHX effectiveness, which is limited due to the discharge temperature of the modeled compressor.

Fig. 12 compares R-1234ze(E) and R-134a for each scenario. Notably, R-1234ze(E) demonstrates a higher COP in most scenarios, except for scenario 1 (TSC configuration), scenario 4, and scenario 6. R-134a performs better in lower temperature ranges than R-1234ze(E) and R-1234yf, whereas R-1234ze(E) outperforms at higher temperatures.

For instance, in scenario 2, the COP reaches 5.94 with R-1234ze(E), while it attains 5.15 with R-134a, reflecting a 15.46% increase in performance for R-1234ze(E). From an energy perspective, R-1234ze(E) showcases superior performance at higher temperatures and significantly lower GWP. For scenario 5, Mateu-Royo et al. [11] show similar COP for similar conditions considering district heating; nevertheless, for similar conditions to scenario 1 SS, the COP differs significantly, being in this paper higher. The compressor efficiency in each scenario is different; consequently, for scenario 1, SS is higher than in scenario 5; this can be observed in Fig. 13. Additionally, Mateu-Royo et al. [11] use an air source heat pump (ASHP) whose performance depends on ambient temperature, in this paper, a water-to-water heat pump is used.

When it comes to the water-to-water heat pump comparison, Pietro et al. [18] made an experimental analysis of R-1234ze(E) for a range of heat source temperatures and determined heat sink temperatures, there are two conditions similar to scenarios 3 and 4; they present a COP 1.5 and 3.1 respectively without IHX, in this paper, the COP is higher because does not take into account the pressure drop and the heat transfer to the surroundings; furthermore the experiment conditions and the compressor efficiency difference must be considered. Also, Molinaroli et al. [19] made a similar analysis as [18], and for a similar case to scenario 6 with a lower compression ratio, their experiment presented a COP value of 1.8 with an SS system. This result shows that to improve the operational performance, a TSC is needed, particularly for high

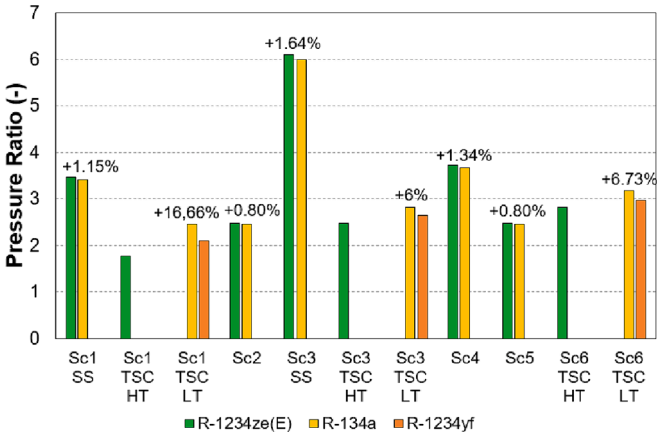

Fig. 8. Pressure ratio comparative between R-1234ze(E), R-134a and R-1234yf.

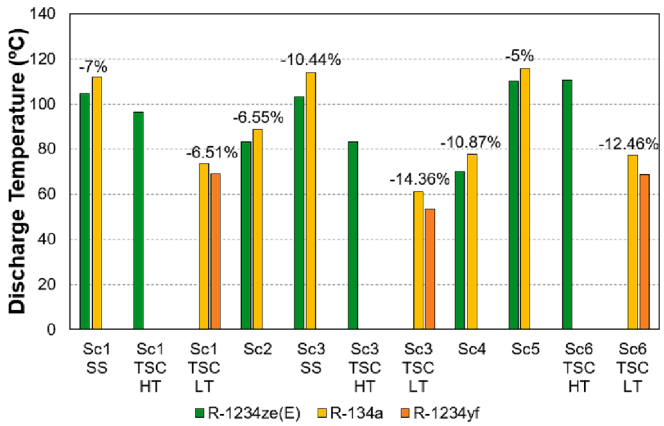

Fig. 9. Discharge temperature comparative between R-1234ze(E), R-134a and R-1234yf with IHX.

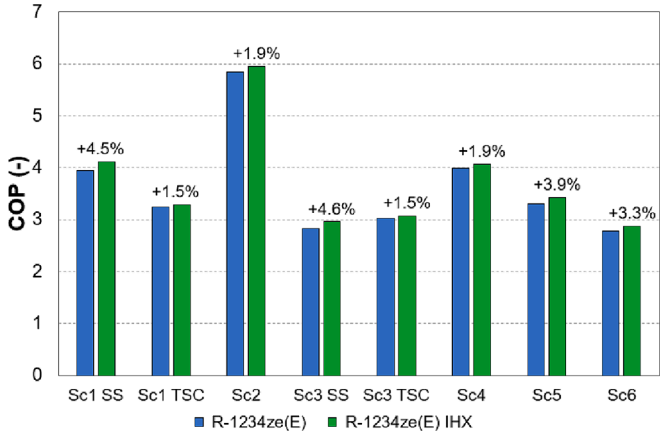

Fig. 10. COP comparative with and without IHX for R-1234ze(E).

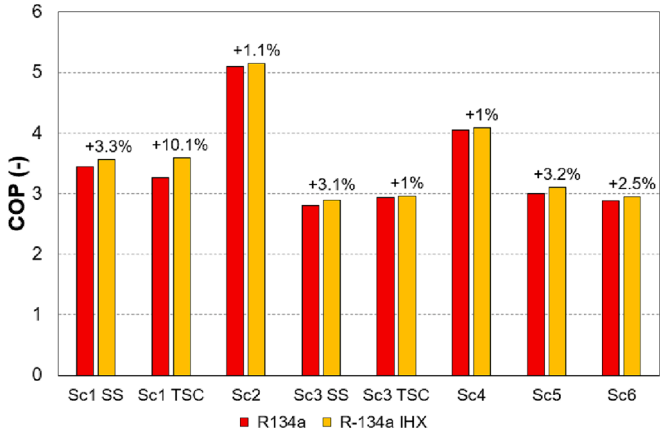

Fig. 11. COP comparative with and without IHX for R-134a.

compression ratio scenarios. In this paper, scenario 6 achieves higher COP (2.87) even with a higher compression ratio because it uses cascade configuration and does not consider the conditions mentioned before for scenarios 3 and 4.

Finally, regarding efficiency comparison, Fig. 13 compares compressor efficiency between R-1234ze(E) and R-134a within each scenario. For TSC LT, R-134a is compared with R-1234yf. The arrangement of scenarios in the figure is based on their evaporating temperatures, starting with Sc3 TSC LT at a 2 °C evaporating

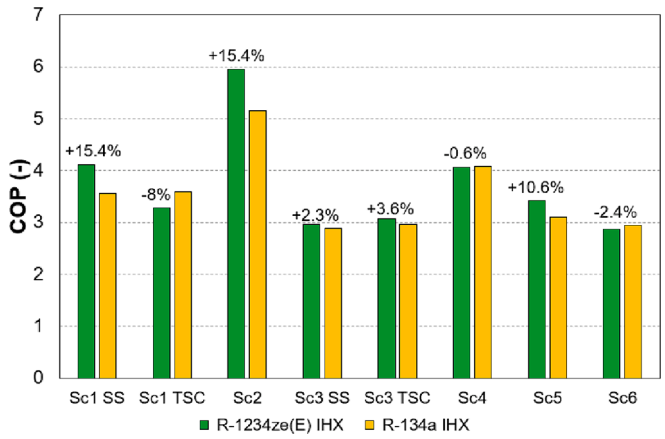

Fig. 12. COP comparative with and without IHX between R-1234ze(E) and R-134a.

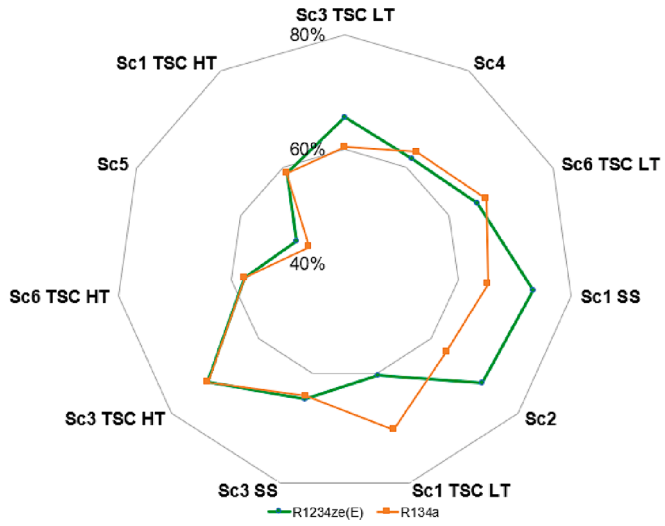

Fig. 13. Compressor efficiencies comparative between R-1234ze(E) and R-134a for each scenario.

temperature and concluding with Sc1 TSC HT at a 55 °C evaporating temperature. The results observed are because the compressor efficiencies are computed by utilizing both the theoretically calculated power and the actual power provided by the manufacturer's software.

Scenarios Sc1 SS, Sc2, and Sc3 TSC HT demonstrate the highest compressor efficiency, attributed to their evaporating temperatures of 30 °C for Sc1 SS and Sc2, and 35 °C for Sc3 TSC HT. The corresponding condensing temperatures are 80 °C for Sc1 SS, and 65 °C for Sc2 and Sc3 TSC HT. Whereas scenario 5 exhibits the lowest efficiency, it features an evaporating temperature of 50 °C and a condensing temperature of 90 °C, leading to very high suction and discharge temperatures for the compressor.

4.2. Carbon footprint analysis

On the one hand, a carbon footprint comparison is conducted among scenarios utilizing R-1234ze(E) and R-134a in Spain, France, and Sweden; taking into consideration the variations in the electrical mix among these countries, the emission factor of each country is 0.165 $kgCO_2$ kWh^{-1} for Spain, 0.058 $kgCO_2$ kWh^{-1} for France and 0.009 $kgCO_2$ kWh^{-1} for Sweden [20]. On the other hand, a comparison between the scenarios and a conventional boiler will be done to evaluate the potential reduction in emissions.

The TEWI analysis needs a set of assumptions (Eq (1)). The leakage ratio (L_a) was determined utilizing data provided by the Australian Institute of Refrigeration [21], with an intermediate leakage ratio of 7% being adopted for this study. The system's operational lifespan (n) has been set at 15 years [22]. The refrigerant charge (m) has been estimated based on the condenser's kilowatt (kW) rating. Given that $\dot{Q}_k$ is 100 kW for all scenarios, the charge was calculated as 0.7 kg kW^{-1}. Consequently, for a 100 kW, the refrigerant charge would be 70 kg. The same principle applies to TSC configurations, with 0.7 kg kW^{-1} selected for each circuit. The refrigerant recycling factor (α) has been determined according to the Australian Institute of Refrigeration [21]. Given that the load is less than 100 kg, a factor of 0.7 has been considered in this context.

$$TEWI = GWP\ m\ L_a\ n + GWP\ m\ (1-\alpha) + (E_a\ \beta\ n) \quad (1)$$

Fig. 14 presents a comparative analysis between R-1234ze(E) and R-134a across different scenarios in Spain. The figure shows that R-1234ze (E) exhibits lower emissions than R-134a, attributable to its lower GWP and superior performance in moderately-high temperature scenarios. Notably, scenario 2 displays the lowest emissions at 358 tCO_2e, whereas scenario 6 records 740.36 tCO_2e for R-1234ze(E). This disparity can be attributed to the performance difference between scenarios 2 and 6, with scenario 6 exhibiting the lowest COP at 2.87. In all scenarios, R-134a consistently emits more than R-1234ze(E). Therefore, from an environmental perspective, R-1234ze(E) demonstrates significantly lower emissions than R-134a. Moreover, it is noteworthy that the tCO_2e values may vary based on the country, as illustrated in Fig. 15 for France and Fig. 16 for Sweden.

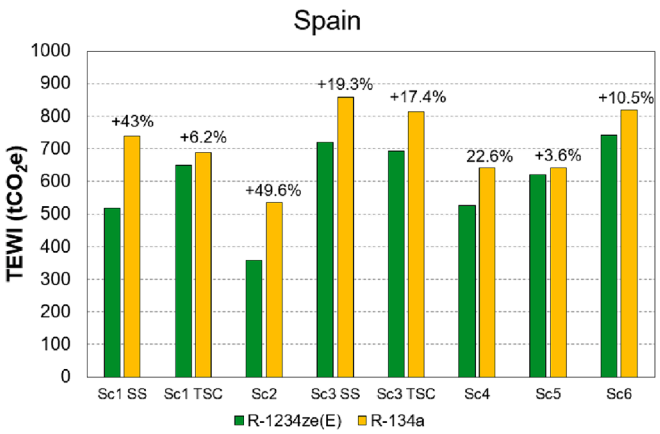

Fig. 14. Emissions comparative between R-1234ze(E) and R-134a for every scenario in Sapin.

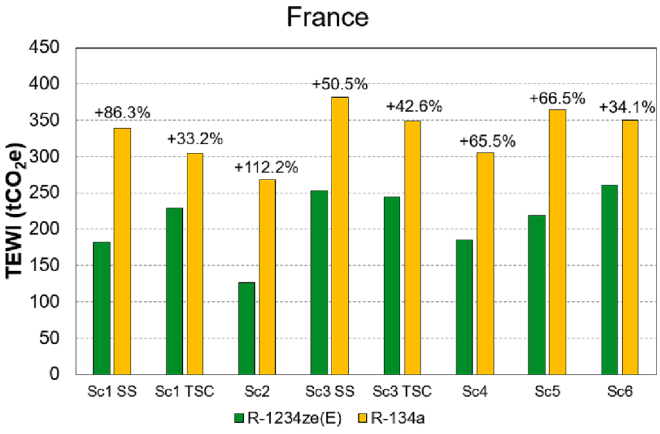

Fig. 15. Emissions comparative between R-1234ze(E) and R-134a for every scenario in France.

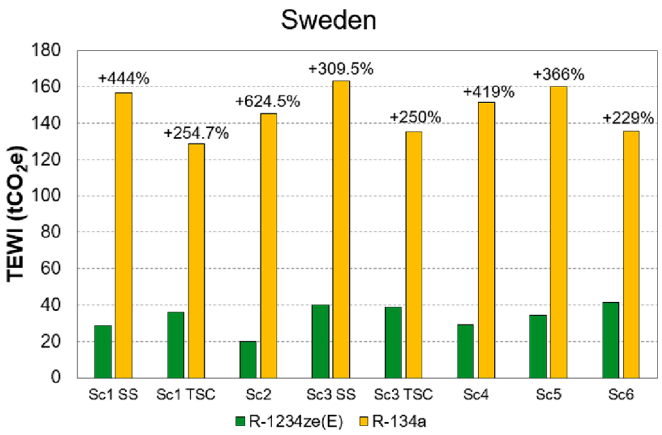

Fig. 16. Emissions comparative between R-1234ze(E) and R-134a for every scenario in Sweden.

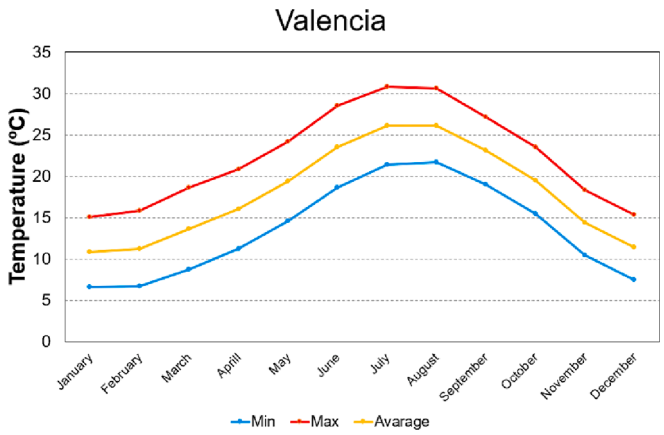

Fig. 17. Ambient temperature in Valencia over the year [28].

The observed difference in emissions between R-1234ze(E) and R-134a is particularly pronounced due to variations in emissions factors between countries, resulting in a more significant difference in direct emissions. In France, scenario 2 emissions are 126.22 tCO_2e, whereas in Sweden are 20.06 tCO_2e. This discrepancy delineates the influence of regional emissions factors on the environmental impact of different scenarios.

It is essential to consider those results because Mateu-Royo et al. [11] made a TEWI analysis for the same countries, and they obtained opposite results. In their case, Sweden emits the maximum and Spain the least; this is because they use ASHP in their study. Therefore, their heat pump depends on the ambient temperature, and as Sweden has the lowest ambient temperature, the ASHP consumes more energy than in higher ambient temperatures. In this paper, a water-to-water heat pump, whose COP and TEWI do not have a dependency on the ambient temperature is used, and this is a significant advantage of this heat pump; consequently, in this case, the emission factor is the parameter that makes TEWI different in those three countries.

To compare scenarios and conventional boilers, the investigation will be conducted in Spain, specifically in Valencia. Valencia was selected as the study location because it is appropriate to represent one of the three European climates, specifically the warmer climate, as outlined in the European Directive 2010/30/EU [23].

The ASHP will be employed in the environmental comparison of scenarios three and four due to the application of the scenarios (simultaneous production of heating and cooling). Consequently, they will be compared with a conventional boiler and chiller. It is important to note that for scenarios three and four, the emissions of the chiller will be added to those of the boiler. The cooling production is designated for a data cooling center, and the ambient temperature was computed using Fig. 17, accounting for the 2 °C evaporation in both scenarios.

The chiller will operate when the ambient temperature exceeds 2 °C. Since ambient temperatures are consistently above 2 °C each month, the chiller is expected to operate throughout the year, except for scheduled maintenance downtime. The condensation temperature will be determined as the average temperature over the year plus 10 °C, resulting in a chiller condensing temperature of 27.95 °C.

On the one hand, Fig. 18 compares HP with a conventional boiler for scenarios exclusively dedicated to heating production. All scenarios exhibit a notable reduction in emissions, with scenario 2 demonstrating the most minor emissions (358 tCO_2e) and the most substantial emission reduction. The emissions from the boiler were computed based on a conventional natural gas boiler with an efficiency curve provided by the manufacturer. The boiler emissions were projected over 15 years, the same as HP. The emission factor utilized is 0.163982 $kgCO_2e$, given by the Spanish Ministry for Ecological Transition [24]. In this context, the

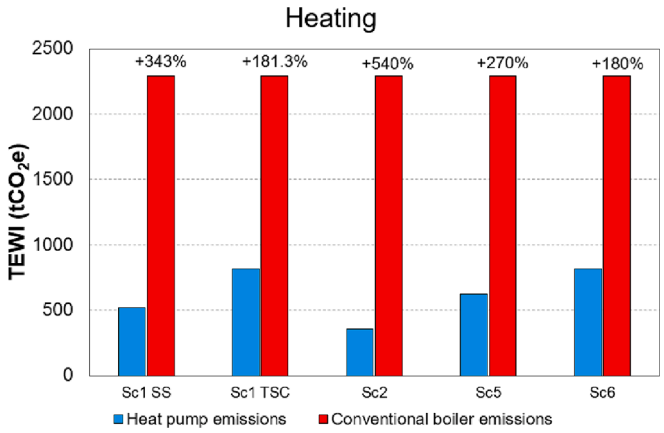

Fig. 18. Emission comparative between HP and conventional boiler for heating.

boiler emissions reach 2290.95 tCO_2e for scenarios 1, 2, 5, and 6. Note that the emissions of the boiler for those scenarios are the same; this is because the temperature range of those four scenarios barely changes the efficiency of the boiler according to the efficiency curve given by the manufacturer.

On the other hand, Fig. 19 compares combined heating and cooling scenarios. Similar to the previous analysis, scenario 3, with its configurations, and scenario 4 exhibit substantial reductions in emissions. In this instance, the combined emissions from the boiler and chiller reach

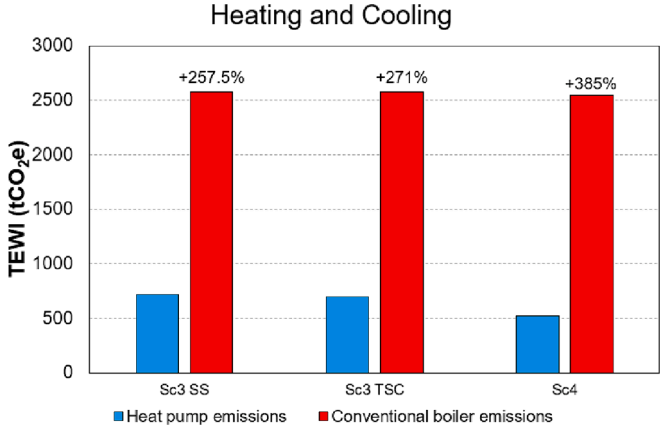

Fig. 19. Emission comparative between HP and conventional boiler for heating and cooling.

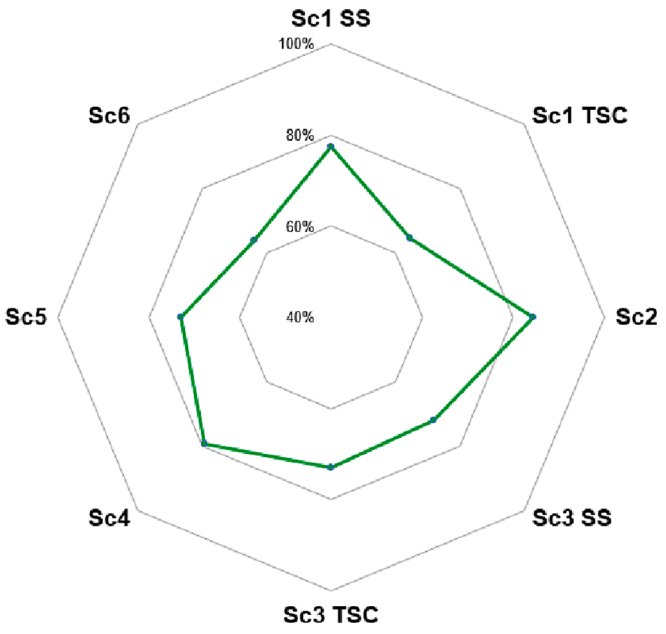

Fig. 20. CO_2 equivalent emissions reduction achieved by employing a heat pump instead of a natural gas boiler.

2573.91 tCO_2e for scenario 3 and 2543.28 tCO_2e for scenario 4. In this case, the boiler's emissions for scenario 4 are different from those of scenario 3 because scenario 4 temperature is lower than scenario 3, which means the boiler's efficiency is increased.

Fig. 20 illustrates the percentage reduction in emissions for each scenario. Scenario 2 demonstrates the most important reduction, with emissions reduced by 84.37%, whereas scenario 6 exhibits the most minor reduction, with emissions reduced by 64.28%.

The results derived from Fig. 20 are attributed to the COP of each scenario. With a constant $\dot{Q}_k$ of 100 kW for all scenarios, the variation in COP results from the actual power consumed by the compressor in each scenario. In Spain, TEWI is primarily influenced by the power consumption. Therefore, scenario 2 demonstrates the highest COP, indicating the lowest TEWI, while scenario 6 exhibits the lowest COP, signifying the highest TEWI. Fig. 21 visually represents this relationship for each scenario, illustrating that higher COP corresponds to lower TEWI and vice versa.

Also, Mateu-Royo et al. [11] conducted emission reduction using a heat pump instead of a boiler; in their paper, there are similar cases to

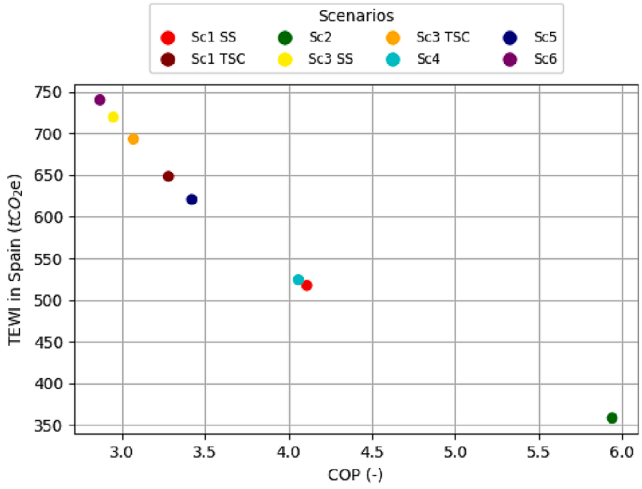

Fig. 21. Comparative between TEWI and COP for each scenario.

scenarios 1 and 5, comparing them to this paper, scenario 5 presents similar emissions reduction. Nevertheless, scenario 1 emissions reduction differs, achieving higher emissions reduction in this paper. Contrasting the results of this paper and Mateu-Royo et al. [11] paper, it is observed that ASHP and water-to-water heat pump performance may differ, even if the conditions are similar. The results obtained in this paper show the promising performance of integrating water-to-water heat pumps into DHC networks.

4.3. Economic analysis

In this section, an economic analysis of the HP for all six scenarios, each with its distinct configurations, will be done in Spain. A comparative evaluation is made between the HP and boiler, and in the cases of scenarios 3 and 4, a chiller as well. The economic evaluation of the HPs is divided into capital expenditure (CAPEX) and OPEX.

On the one hand, the CAPEX englobe the expenses associated with each component of the HP and the boiler, as illustrated in Fig. 22. The scenarios exhibiting the lowest CAPEX are scenarios 2 and 1, while the TSC scenarios prove to be the most expensive due to the costs of their components. Notably, the boiler offers the least CAPEX. A plate heat exchanger is employed for each condenser, evaporator, and cascade heat exchanger. The pricing details are derived using Eq (2) [25]. The price of the three components (C_{HX}) depends on the surface area of the condenser, evaporator, and cascade heat exchanger.

$$C_{HX} = \left(1397\left(A_{cond}^{0.89} + A_{evap}^{0.89}\right) + 2382.9\, A_{CHX}^{0.68}\right) 0.91{\cdot}2.065 \tag{2}$$

The equation is multiplied by 0.91 to convert the prices into euros and further scaled by 2.065 to adjust for the price update to 2022. However, determining prices requires knowledge of the heat exchanger's area. The areas were calculated using Eq (3). The heat transfer coefficient (U) utilized in this instance is set at 1000 kW m^{-2} K^{-1} [25]. The rest of the components were selected from the manufacturer to obtain their cost.

$$A_{HX} = \frac{\dot{Q}_{HX}}{U\ \Delta T_{LMTD}} \tag{3}$$

On the other hand, OPEX depends on the energy consumed by the HPs, boiler, and chillers. For the HPs and chillers, the cost is due to electricity consumption, while for the boiler, it corresponds to the cost of natural gas. The installation has a life cycle of 15 years, during which electricity and natural gas prices are subject to change. This investigation considers the price evolution over fifteen years (from 2007 to 2022) in the OPEX. During the fifteen years, the Electricity prices range from 0.13 to 0.2957 € kWh^{-1}, and the gas prices range from 30 to 120 € MWh^{-1} [26]. Notably, due to the energy consumption of the HPs in this study, the considered prices belong to band IB.

The OPEX has been calculated using the average price because, for the majority of the fifteen years, the price is around the average; the maximum price occurs when there is a particular crisis in the respective sector. Fig. 23 shows the annual OPEX for scenarios exclusively compared with the boiler. In this context, the OPEX of the boiler remains consistent across all scenarios because, as mentioned before, its efficiency barely changes for those conditions. Fig. 23. Scenario 2 demonstrates the lowest operating costs due to its superior performance.

Fig. 24 illustrates OPEX for scenarios compared to the chiller and boiler. The boiler for scenario 4 presents a different OPEX from scenario 3 because it presents higher efficiency. In the economic viability study, the CAPEX costs of the chillers will be combined with those of the boiler when comparing scenarios 3 and 4. A similar approach will be taken with the OPEX.

As observed in Figs. 23 and 24, some scenarios have a big potential to economically replace boilers because they present lower OPEX than boiler or boiler plus chiller, which allows a promising payback period (PBP). Lu et al. [27] also used this strategy for high-temperature cascade

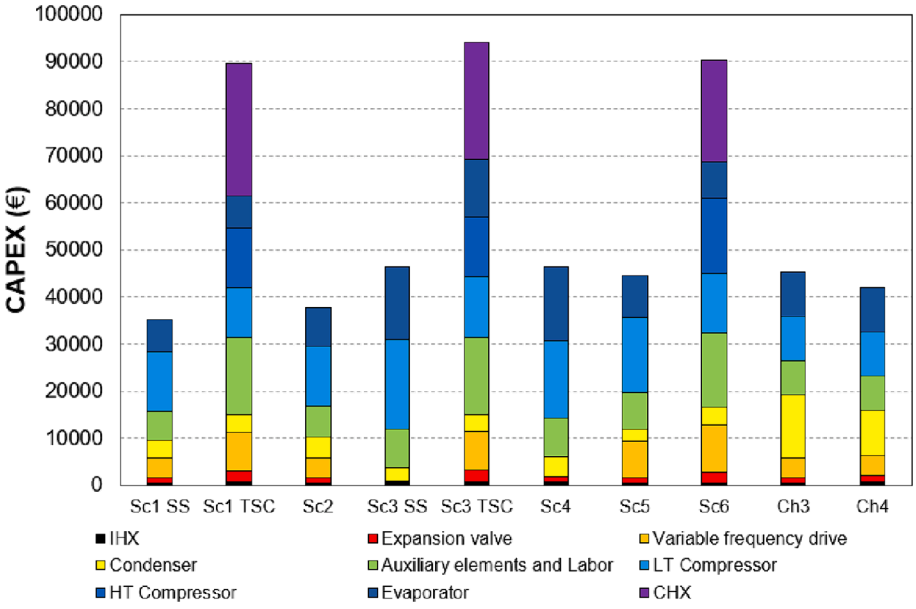

Fig. 22. CAPEX of the scenarios, chillers, and boiler.

heat pumps for steam generation, and they obtained a promising PBP for their conditions.

Fig. 25 illustrates the comparison between the Total Cost of Ownership (TCO) and emissions of the HP for each scenario over a 15-year life cycle. The comparison reveals that higher emissions correspond to a higher TCO, a consequence of the HP performance. As shown in Fig. 21, a lower TEWI indicates higher performance. This explains why scenario 2 exhibits a TCO of approximately half a million euros, whereas scenario 6 has a TCO of around one million two hundred thousand euros.

Economic viability is evaluated based on the feasibility of using HP instead of a natural gas boiler. To calculate economic viability, the net present value (NPV) will be calculated using Eq. (4). Additionally, the internal rate of return (IRR) will be determined using Eq. (5), and the PBP will be calculated using Eq. (6). The initial investment (I_o) is the CAPEX of the scenarios. The I_o of the boiler and chillers are zero because it's assumed to exist already. For calculating the cash inflow (CF_t), the profit is determined as the OPEX of the boiler or the boiler plus chiller minus the cost of the HP. The discount rate (r) is computed taking into account the Consumer Price Index (CPI) in Spain, which stands at 3.20% as of May 2023.

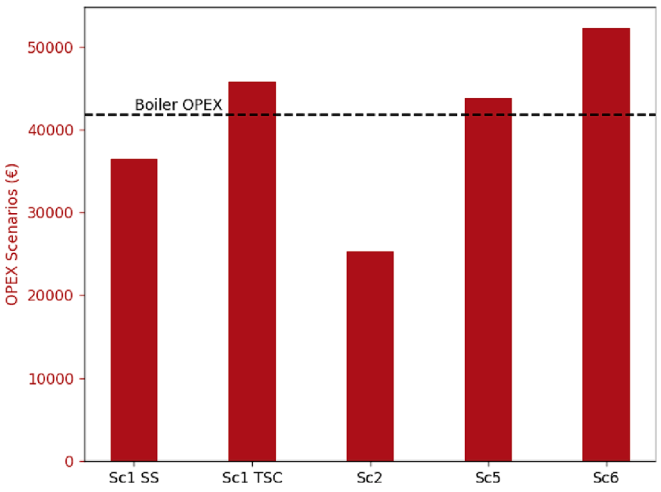

Fig. 23. OPEX of the scenarios compared with the boiler.

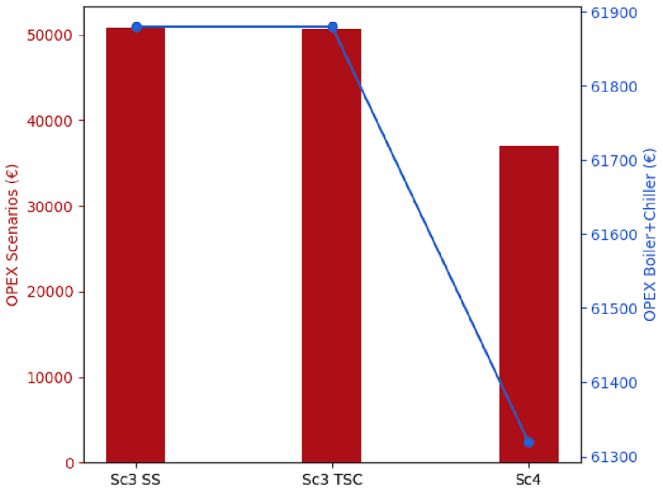

Fig. 24. OPEX of the scenarios compared with boiler and chiller.

$$NPV = \sum \left(\frac{CF_t}{(1+r)^t} \right) - I_O \tag{4}$$

$$0 = \sum \left(\frac{CF_t}{(1+IRR)^t} \right) - I_O \tag{5}$$

$$PBP = \frac{I_o}{Avarage\ Annual\ cash\ InFlow} \tag{6}$$

Table 4 presents the Net Present Value (NPV), Internal Rate of Return (IRR), and Payback Period (PBP) for financially viable scenarios. Scenarios 1 (TSC), 5, and 6 are considered unfeasible due to their elevated energy consumption, leading to OPEX surpassing those of the boiler. In this paper the TSC configurations, except scenario 3, are not economically feasible as opposed to Lu et al. [27] due to the conditions and compression ratio of scenarios 1 TSC and 6 TSC, they present high energy consumption and high CAPEX surpassing the boiler in all aspects. Regarding the TSC configuration in scenario 3, CAPEX is double compared to the SS configuration, consequently the SS configuration is more viable. Notably, scenarios 3, SS, and 4 yield favorable results as

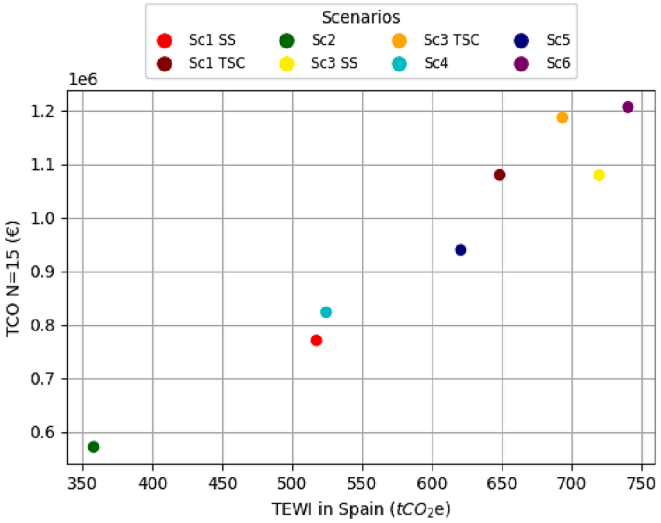

Fig. 25. Comparative between TEWI and TCO for N = 15 years.

Table 4
NPV, IRR, and PBP for financially viable scenarios.

Scenarios	NPV (€)	IRR	PBP (years)
Scenario 1 SS	34680.01	17.9%	4.70
Scenario 2	136371.74	39.4%	2.18
Scenario 3 SS	77942.78	23.6%	3.67
Scenario 4	205635.29	43.6%	1.96

they are compared to a boiler plus chiller. The inclusion of a chiller introduces additional OPEX, amplifying the comparative cost. This shows the advantage that HP demonstrates in the simultaneous production of heating and cooling.

Furthermore, scenario 2, with its favorable conditions, offers low CAPEX and OPEX. Its minimal energy consumption results in a remarkably short payback period of 2.18 years. In contrast, scenario 1 (SS) exhibits the least economic viability indicator due to its moderately-high temperature condition (T_k= 90 °C). However, it remains a viable alternative for applications requiring high temperatures.

4.4. Global analysis

Table 5 comprehensively summarizes the operational, carbon footprint, and economic analyses. Among the six scenarios, scenario 2 appears to be the most promising one. This scenario presents the highest COP, the lowest emissions, and a favorable PBP indicator.

5. Conclusion

This study proposes the implementation of an HP system utilizing R-1234ze(E) as an alternative to traditional natural gas boilers. The selected refrigerant, R-1234ze(E), offers the advantages of a low GWP and appropriateness for moderately-high temperature applications, being a viable substitute for conventional natural gas boilers in HP systems. The investigation contains six distinct scenarios, each one presenting a specific connection to the DHN or DHC, resulting in unique operating conditions for each scenario.

These scenarios vary in their utilization of heat for heating to DHN or for simultaneous heating and cooling for DHC, as well as boiler applications. Due to these diverse conditions, certain scenarios are examined with an SS configuration, whereas others employ a TSC configuration.

Three analyses have been conducted in this study: an operational analysis, a carbon footprint analysis, and an economic analysis:

- First, the Operational analysis reveals that incorporating an IHX into the HPs improves its COP. Scenario 2, with the lowest compression ratio, achieves the highest COP at 5.95, whereas scenario 6, with the highest compression ratio, records the lowest at 2.87. This implies that scenario 2 consumes significantly less energy than scenario 6, given a constant heat load at the condenser ($\dot{Q}_k$) of 100 kW for all scenarios. Other scenarios also demonstrate accurate COP values suitable for their respective applications. The analysis shows that the TSC configurations in scenario 1 underperform SS; in the case of scenario 3, it is the opposite. Compared to R-134a, most scenarios surpass its COP, especially those featuring moderately-high temperature conditions.
- Secondly, the environmental analysis, conducted with an IHX, indicates that scenario 2 exhibits the lowest emissions, reaching 358.02 tCO_2e in Spain; in contrast, scenario 6 shows the highest emissions at 740.36 tCO_2e due to its substantial energy consumption. The lower GWP of R-1234ze(E) compared to R-134a results in lower emissions across all scenarios. Additionally, calculating the TEWI for different countries reveals that when the emission factor is lower, the emissions are reduced and the direct emissions appear more relevant, leading to significant emission differences between R-1234ze (E) and R-134a. Compared to the natural gas boiler, all scenarios exhibit a crucial emissions reduction. Scenario 2, with the lowest emissions, also demonstrates the highest emissions reduction at 84.37%, while scenario 6, with the lowest reduction, still achieves 64.28%.
- Finally, the economic analysis indicates that TSC configurations have the highest CAPEX due to their additional components. As seen in scenarios 1 and 2, the SS configurations exhibit the lowest costs at 35160.91 € and 37717 €, respectively. Regarding OPEX, scenario 2 stands out with the lowest cost, reflecting its superior operational performance, at 25274.91 €, while scenario 6 records 52286.49 €. The economic viability study shows that only scenario 1 (SS), scenario 2, scenario 3 (SS), and scenario 4 are economically viable. Due to their high OPEX, the remaining scenarios cannot compete with the boiler in terms of affordability. Scenarios 4 and 2 show the most favorable outcomes with PBP of 1.96 and 2.18 years, respectively.

In summary, the paper shows that scenario 1 is a viable solution in district heating for industrial processes, scenario 2 is a viable solution for other applications of district heating with high energy efficiency, and scenarios 3 and 4 are viable solutions for simultaneous production heat and cooling for district heating and cooling networks. All scenarios are

Table 5
Summary of the analysis results for each scenario.

Scenario	Configuration	COP (−)	Emissions in Sapin (tCO_2e)	PBP (years)
Scenario 1	SS	4.11	517.47	4.70
	TSC	3.28	648.57	–
Scenario 2	SS	5.94	358.02	2.18
Scenario 3	SS	2.95	719.82	3.67
	TSC	3.07	693.52	–
Scenario 4	SS	4.06	524.35	1.96
Scenario 5	SS	3.42	620.76	–
Scenario 6	TSC	2.87	740.36	–

viable environmentally and economically compared to natural gas boilers (except scenarios 5 and 6 in the economic case). This makes the moderately-high-temperature heat pumps in the first four scenarios more attractive in the market than the low-cost natural gas boiler.

This paper is limited to a theoretical simulation using manufacturer data and boundary conditions considered. In practice, conditions may differ from simulated results. In practical applications, factors such as compressor efficiency, pressure drop, heat transfer to the surroundings, and operational limitations can introduce differences that are not fully captured in theoretical models. Consequently, for future work, the scenarios considered in this paper will be experimented at the laboratory using a prototype heat pump based on the configurations employed in this paper to evaluate the operational and carbon footprint feasibility. Furthermore, other refrigerants will be tested, such as mixtures of HFO with low GWP; in this case, the conditions will be identical or nearly identical depending on the thermodynamical properties of the mixtures. Also, a sensitivity analysis will be conducted, and uncertainties will be considered.

CRediT authorship contribution statement

Ghad Alarnaot Alarnaout: Writing – review & editing, Writing – original draft, Visualization, Software, Methodology, Formal analysis, Data curation, Conceptualization. **Joaquín Navarro-Esbrí:** Supervision, Methodology, Formal analysis, Conceptualization. **Adrián Mota-Babiloni:** Writing – original draft, Project administration, Methodology, Investigation, Funding acquisition.

Declaration of competing interest

The authors declare the following financial interests/personal relationships which may be considered as potential competing interests: Joaquin Navarro Esbri reports financial support was provided by University Jaume I. Adrian Mota Babiloni reports financial support was provided by State Agency of Research. If there are other authors, they declare that they have no known competing financial interests or personal relationships that could have appeared to influence the work reported in this paper.

Data availability

Data will be made available on request.

Acknowledgements

This scientific publication is part of the project UJI-B2022-65 and UJI. > LAB IMPULS/2022/02, funded by Universitat Jaume I. Adrián Mota-Babiloni acknowledges contract IJC2019-038997-I, funded by MCIN/AEI/10.13039/501100011033.

References

[1] European Commission. (2023). Heat pumps-action plant to accelerate roll-out across the EU https://energy.ec.europa.eu/topics/energy-efficiency_en.
[2] Gerard, F., Guevara Opinska, L., Smit, T., Rademaekers, K., & Trinomics. (2021). Policy Support for Heating and Cooling Decarbonisation. https://op.europa.eu/en/publication-detail/-/publication/f5118ffc-eabd-11ec-a534-01aa75ed71a1/language-en.
[3] Barco-Burgos J, Bruno JC, Eicker U, Saldaña-Robles AL, Alcántar-Camarena V. Review on the integration of high-temperature heat pumps in district heating and cooling networks. Energy 2022;239. https://doi.org/10.1016/j.energy.2021.122378.
[4] Ma, Z., Knotzer, A., Billanes, J. D., & Jørgensen, B. N. (2020). A literature review of energy flexibility in district heating with a survey of the stakeholders' participation. In *Renewable and Sustainable Energy Reviews* (Vol. 123). Elsevier Ltd. DOI: 10.1016/j.rser.2020.109750.
[5] Buffa, S., Cozzini, M., D'Antoni, M., Baratieri, M., & Fedrizzi, R. (2019). 5th generation district heating and cooling systems: A review of existing cases in Europe. In *Renewable and Sustainable Energy Reviews* (Vol. 104, pp. 504–522). Elsevier Ltd. DOI: 10.1016/j.rser.2018.12.059.
[6] Lund H, Østergaard PA, Nielsen TB, Werner S, Thorsen JE, Gudmundsson O, et al. Perspectives on fourth and fifth generation district heating. Energy 2021;227. https://doi.org/10.1016/j.energy.2021.120520.
[7] Sayegh MA, Jadwiszczak P, Axcell BP, Niemierka E, Bryś K, Jouhara H. Heat pump placement, connection and operational modes in European district heating. In: Energy and Buildings, Vol. 166. Elsevier Ltd.; 2018. p. 122–44. https://doi.org/10.1016/j.enbuild.2018.02.006.
[8] A.K.S. Al-Sayyab A. Mota-Babiloni J. Navarro-Esbrí Renewable and waste heat applications for heating, cooling, and power generation based on advanced configurations Energy Conversion and Management Vol. 291 2023 Elsevier Ltd 10.1016/j.enconman.2023.117253.
[9] Mateu-Royo C, Mota-Babiloni A, Navarro-Esbrí J, Barragán-Cervera Á. Comparative analysis of HFO-1234ze(E) and R-515B as low GWP alternatives to HFC-134a in moderately high temperature heat pumps. Int J Refrigeration 2021;124:197–206. https://doi.org/10.1016/j.ijrefrig.2020.12.023.
[10] Xiao S, Nefodov D, McLinden MO, Richter M, Urbaneck T. Working fluid selection for heat pumps in solar district heating systems. Sol Energy 2022;236:499–511. https://doi.org/10.1016/j.solener.2022.02.036.
[11] Mateu-Royo C, Sawalha S, Mota-Babiloni A, Navarro-Esbrí J. High temperature heat pump integration into district heating network. Energy Conversion Management 2020;210. https://doi.org/10.1016/j.enconman.2020.112719.
[12] Jiang, J., Hu, B., Wang, R. Z., Deng, N., Cao, F., & Wang, C. C. (2022). A review and perspective on industry high-temperature heat pumps. In *Renewable and Sustainable Energy Reviews* (Vol. 161). Elsevier Ltd. DOI: 10.1016/j.rser.2022.112106.
[13] Hamid K, Sajjad U, Ulrich Ahrens M, Ren S, Ganesan P, Tolstorebrov I, et al. Potential evaluation of integrated high temperature heat pumps: a review of recent advances. Appl Thermal Eng 2023;230. https://doi.org/10.1016/j.applthermaleng.2023.120720.
[14] Sulaiman AY, Cotter D, Wilson C, Kamkari B, Hewitt N. Energetic and exergo-environmental analysis of transcritical high-temperature heat pumps with low GWP refrigerants for industrial waste heat recovery. Int J Refrigeration 2023;156:12–28. https://doi.org/10.1016/j.ijrefrig.2023.09.021.
[15] Klein, S. (2006). Engineering Equation Solver (EES) V10.835 https://www.fchartsoftware.com/.
[16] BITZER. (2020). Retrieved March 7, 2024, from https://www.bitzer.de/es/es/productos/.
[17] BITZER. (2016). Bitzer software V6.17 https://www.bitzer.de/ec/es/tools-archive/software/software/.
[18] Pietro, L., Colombo, M., Lucchini, A., & Molinaroli, L. (2020). Experimental analysis of the use of R1234yf and R1234ze(E) as drop-in alternatives of R134a in a water-to-water heat pump. In *International Journal of Refrigeration*, *115*, 18–27 Elsevier Ltd. DOI: 10.1016/j.ijrefrig.2020.03.004.
[19] Molinaroli L, Lucchini A, Colombo LPM, Bocchinfuso F. First experimental results of the use of R1234yf and R1234ze(E) as drop-in substitutes for R134a in a water-to-water heat pump. J Phys Conf Ser 2020;1599(1). https://doi.org/10.1088/1742-6596/1599/1/012057.
[20] European Environment Agency. (2023). Retrieved January 4, 2024, from https://www.eea.europa.eu/data-and-maps/daviz/co2-emission-intensity-13/#tab-chart_4.
[21] AIRAH, O. (2012). Methods of calculating Total Equivalent Warming Impact (TEWI). Best practice guidelines the Australian institute of refrigeration, air conditioning and heating 2 methods of calculating total equivalent warming impact (TEWI) best practice guidelines. www.airah.org.au.
[22] Staubach D, Michel B, Revellin R. Refrigerant selection from an economic and TEWI analysis of cascade refrigeration systems in Europe based on annual weather data. Appl Therm Eng 2023;230. https://doi.org/10.1016/j.applthermaleng.2023.120747.
[23] EUR-Lex. Directive 2010/30/EU of the European Parliament and of the Council of 19 May 2010 on the indication by labelling and standard product information of the consumption of energy and other resources by energy-related products. Retrieved January 4, 2024, from, https://eur-lex.europa.eu/legal-content/EN/ALL/?uri=CELEX:32010L0030; 2010.
[24] MITECO. (2022). Factores de emisión. chrome-extension://efaidnbmnnnibpcajpcglclefindmkaj/https://www.miteco.gob.es/content/dam/miteco/es/cambio-climatico/temas/mitigacion-politicas-y-medidas/factoresemision_tcm30-479095.pdf.
[25] Staubach D, Michel B, Revellin R. Refrigerant selection from an economic and TEWI analysis of cascade refrigeration systems in Europe based on annual weather data. Appl Therm Eng 2023;230:120747. https://doi.org/10.1016/j.applthermaleng.2023.120747.
[26] Eurostat. (2022). Retrieved January 4, 2024, from https://ec.europa.eu/eurostat/web/main/search/-/search/estatsearchportlet_WAR_estatsearchportlet_INSTANCE_bHVzuvn1SZ8J?text=prices.
[27] Lu Z, Yao Y, Liu G, Ma W, Gong Y. Thermodynamic and economic analysis of a high temperature cascade heat pump system for steam generation. Processes 2022;10(9). https://doi.org/10.3390/pr10091862.
[28] Data C. Clima Valencia. Retrieved January 4, 2024, from, https://es.climate-data.org/europe/espana/comunidad-valenciana/valencia-845/; 2022.
[29] Honeywell | Refrigerants. (2018). Retrieved January 5, 2024, from https://www.honeywell-refrigerants.com/europe/product/solstice-1234ze/.
[30] Honeywell | Refrigerants. (2015). Retrieved January 5, 2024, from https://www.honeywell-refrigerants.com/europe/product/solstice-yf-refrigerant/.
[31] Honeywell | Refrigerants. (2007). Retrieved January 5, 2024, from https://www.honeywell-refrigerants.com/europe/product/genetron-134a/.
[32] ASHRAE. (2017). Fundamentals Inch-Pound Edition. *2017 ASHRAE HANDBOOK*. https://search.worldcat.org/title/989056692.